Contents lists available at ScienceDirect

# Experimental Thermal and Fluid Science

# Experimental determination of the convection heat transfer coefficient in an eccentric annular duct

Daniel Serrano [*], Sergio Sánchez-Delgado, Rafael Pérez-Álvarez, Antonio Acosta-Iborra

*Energy System Engineering Research Group, Thermal and Fluid Engineering Department, Carlos III University of Madrid, 28911 Leganés, Madrid, Spain*

ARTICLE INFO

ABSTRACT

The use of bayonet tube heat exchangers and heaters is widespread in many industrial applications and an improvement in the heat transfer coefficient may provide benefits over other technologies. This work presents novel experimental results about the turbulent convection heat transfer coefficient of air in the annular section of a bayonet tube for two different configurations: concentric and eccentric tubes. For both configurations, the convection heat transfer coefficient was obtained at different air flow rates, therefore, at different Reynolds numbers. In the case of the eccentric configuration, the angular position of the inner tube was varied to determine the circumferential distribution of the local convective heat transfer coefficient. An increase of the convection coefficient was observed for both configurations at higher Reynolds numbers. Concerning the angular position with regard the inner tube, the largest local convective heat transfer coefficient was obtained at the angular position where the distance between the inner and outer tubes was maximum, yielding a value 22.3% higher than in the case of a concentric annular section. All these experimental results were used to propose a new correlation for the local convective heat transfer coefficient as a function of the Prandtl and Reynolds numbers, the eccentricity, and the angular position of the inner tube, with a maximum discrepancy between correlation and experimental data below 10%.

## 1. Introduction

Almost all the thermal processes in the energy generation sector have been optimized in the past due to their significant impact in the plant efficiency and reliability. Thus, even tiny enhancements of the performance of these thermal processes might provide advantages over other technologies. In this framework, several research works focus their attention on this challenge of improving heat transfer process through the use of bayonet tubes in industrial applications such as heat exchangers, boilers, thermal storage systems, nuclear reactors, solar receivers, pharmaceutical or bio-chemicals factories [1,2]. A bayonet tube comprises two tubes, one inside the other. Both tubes split the fluid flow in two counterflow paths: (i) an annular passage, which is formed by the gap between the external tube and the inner tube, and (ii) a circular passage inside the inner tube. Both paths are connected at the top of the tube, where an end-cap blocks the exit of the fluid at this point. Depending on the inner tube position, there are two possible bayonet tube configurations: concentric and eccentric. When the outer and inner tubes have the same geometrical centre, they form a concentric bayonet tube ($\xi = 0$). Otherwise, if the axes of the inner and outer tubes are

separated, i.e., are not coincident, the resulting configuration is an eccentric bayonet tube ($\xi > 0$). Here, the eccentricity is defined as a function of the separation between tube centres, $e$, and the hydraulic diameter of the annular cross-section, $D_h$, as $\xi = e/D_h$. Thanks to the eccentricity, an asymmetry is generated in the flow, which can be used to increase the heat transfer coefficient in the widest gap of the annular cross-section. This fact opens the possibility of further reducing temperature gradients of the tube wall without pressure drop enlargements, which would enhance the thermal efficiency and safe operation of processes such as the cooling of the rods of nuclear reactors [3–5], the extraction of oil and gas [6], the catheterization of arteries [7], heat transfer in close-packed tubular exchangers [8], and cleaning of geothermal wells [9]. Therefore, the study of the fluid flow and heat transfer in bayonet tubes is essential to understand and optimize these systems, especially the flow in the annular cross-section, which is more complex and less abundant in literature than the flow in circular sections. Concerning ducts of annular cross-section, the literature about this topic can be organized into two groups: the characterization of the fluid flow and heat transfer in concentric and eccentric annuli.

The behaviour of the fluid flow and its convection heat transfer inside concentric annular ducts has been studied in many works through

**Nomenclature**

*Latin symbols:*

| | |
|---|---|
| $D_h$ | hydraulic diameter [m] |
| $D_i$ | inner diameter external tube [m] |
| $d_e$ | outer diameter of the internal tube [m] |
| $d_{orifice}$ | diameter of the measurement orifice [m] |
| $e$ | distance between tubes axes [m] |
| G | Adaptation coefficient |
| $Gr$ | Grashof number [–] |
| $h$ | convection heat transfer coefficient [W·m$^{-2}$·K$^{-1}$] |
| $k$ | thermal conductivity [W·m$^{-1}$·K$^{-1}$] |
| $L_c$ | characteristic length [m] |
| $Nu$ | Nusselt number [–] |
| $Pr$ | Prandtl number [–] |
| $q''$ | heat flux [W·m$^{-2}$] |
| $Re$ | Reynolds number [–] |
| $T$ | temperature [°C] |

| | |
|---|---|
| $u$ | velocity [m/s] |

*Greek letters:*

| | |
|---|---|
| $\delta$ | discrepancy [–] |
| $\xi$ | eccentricity [–] |
| $\theta$ | angular position relative to the inner tube |
| $\rho$ | density [kg/m$^3$] |
| $\mu$ | dynamic viscosity [Pa·s] |

*Subscripts*

| | |
|---|---|
| air | air |
| conc | concentric case |
| exp | quantity obtained from experimental measurements |
| fd | fully developed conditions |
| m | mean quantity |
| nd | non-developed conditions |
| $\theta$ | local variable |
| $\theta, D_h$ | local variable evaluated at the hydraulic diameter |

numerical analysis for different orientations of the duct (horizontal [10] and vertical duct [11,12]) and, for various fluids (air [10,13], water [12], oil [14] and even nanofluids [15,16]). Besides, different mechanisms of convection heat transfer in annular ducts have been analysed in the literature, i.e., natural [10,13], mixed [12] and forced convection [14]. These studies have been used to report how the heat transfer, which is usually represented through the Nusselt number ($Nu$) or the convection coefficient ($h$), is affected by the operating conditions. Kaneda et al. [17] and Yu et al. [18] performed a different numerical study, developing predictive expressions from theoretical considerations for the shear stress, velocity and $Nu$ in a uniformly heated concentric annulus. In contrast, numerical studies concerning eccentric annular ducts are much less frequent. For example, Nikitin et al. [19] performed a direct numerical simulation of the turbulent flow and heat transfer in an eccentric annulus while Nobari and Asgarian [20] numerically investigated the mixed convection in a vertical eccentric annulus.

In addition, different experimental studies have also been carried out to evaluate the convection coefficient and the heat transfer. Mohammed et al. [21] studied the mixed convection heat transfer under laminar conditions ($200 < Re < 1000$ and $6.2 \cdot 10^5 < Gr < 1.2 \cdot 10^7$) in a horizontal concentric annulus with a constant heat flux in the inner tube. Kim et al. [22] also analysed the mixed convection but in a vertical concentric annulus. Farias et al. [2] evaluated the Nusselt number for a viscoplastic liquid under laminar conditions in a horizontal concentric annulus. Dirker and Meyer [23] developed an experimental study of convective heat transfer in concentric annuli to predict the Nusselt numbers and their dependence with annular diameter ratios. Gnielinski [24] developed different correlations for the heat transfer coefficient for turbulent flow in concentric annular ducts, considering the effect of the annular diameter ratio. Jonsson and Sparrow [25] characterized the features of the turbulent flow field and pressure drop for an eccentric annular duct, varying the tube eccentricity from a concentric configuration to an extreme eccentric configuration in which the walls of the external and the inner tubes were in contact. Nouri et al. [26] measured the flow velocity components and their shear stresses for Newtonian and non-Newtonian flows in concentric and eccentric annular ducts. Choueiri and Tavoularis [27] analysed experimentally how gap instability is started in eccentric annular channels and how a vortex street is generated and evolve laminar, transitional and turbulent flow conditions . This work was completed with additional measurements in [28], where the effects of the eccentricity, Reynolds number, the inlet conditions, and the radius ratio on the gap instability and gap vortex streets were discussed. Hosseini et al. [29] studied the natural convection in an annular duct in which the eccentricity was varied from zero (concentric)

to $\xi = 0.5$.

None of the above-mentioned experimental works directly or indirectly measured the distribution of the local convective heat transfer coefficient along the perimeter of the eccentric annular ducts. Just an average value of the convective heat transfer coefficient is reported in some of these or other works as far as the authors are concerned. However, knowledge of the local convective heat transfer coefficient in annular ducts would help to better understand and optimize these systems and will be also very useful to validate numerical simulations. Due to the limited number of studies in the literature to experimentally characterize the local convective heat transfer process in eccentric annular ducts, this work presents a novel methodology to experimentally measure the local value of the convective heat transfer coefficient on the inner surface of the outer tube of annular ducts. The variation of this coefficient with the Reynolds number of an internal turbulent flow of air is obtained for concentric and eccentric annular ducts. The circumferential distribution of the local convective heat transfer coefficient in an eccentric annular duct at various air flow velocities is determined using, for the first time, experimental measurements. Additionally, an experimental correlation of the local Nusselt number as a function of the Reynolds number and the angle position, is proposed based on the obtained experimental data.

## 2. Experimental methodology

### 2.1. Experimental setup

The experiments were carried out in a lab-scale facility in which ambient air was passed through the cross-section of an annular duct representing a bayonet tube. A heating system is located in the middle of the height of the bayonet tube, where the distance from the air inlet is enough to ensure a hydraulic development of the flow in turbulent conditions. The heating system introduces heat through only a portion of the external tube, where the local temperature is measured. The experimental apparatus was made up of four different sub-systems: bayonet tube, heating & measurement region, power supply and image acquisition system. Fig. 1a-b show a picture of the whole setup while Fig. 1c-f show different details of the subsystems.

As mentioned above, the bayonet system consisted of two tubes of smooth surfaces: an external one made of methacrylate of 5.4 cm inner diameter ($D_i$, red dashed-line in Fig. 1c and e), and an internal one made of aluminium of 2.2 cm outer diameter ($d_e$, blue dashed-line in Fig. 1c and e). In this work, a concentric configuration (nominal case) and an eccentric configuration have been analysed. The centre of the internal
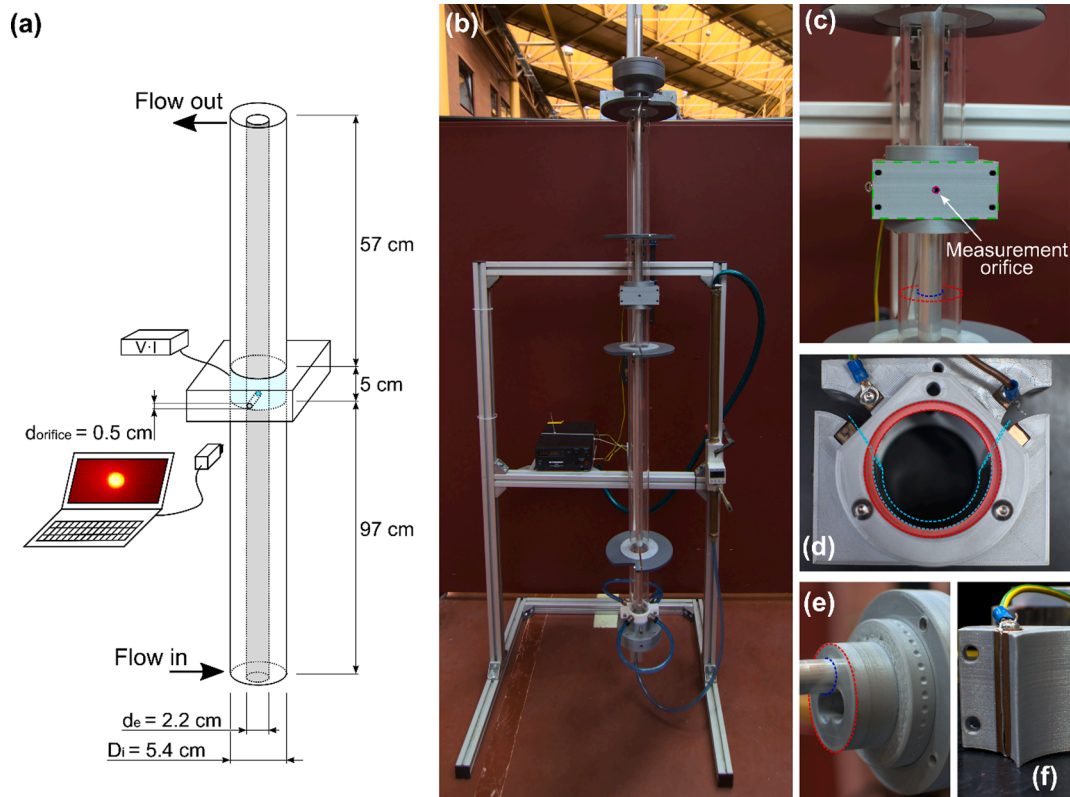
**Fig. 1.** Experimental setup: a) experimental facility scheme; b) experimental facility; c) annular section (red and blue dashed-lines denote the inner and external tube perimeters) and heating & measurement region (green and purple dashed-lines); d) detail of the heating film (light blue dashed-line), connections and adjustment of the external tube in the upper and bottom parts of the measurement region (red shaded area; e) detail of the eccentricity and positioning device; and f) detail of the indium wire for a uniform current distribution.

tube was moved away 1.4 cm from the central position to produce a smooth eccentricity of $\xi = 0.44$ in the annular duct.

The heating & measurement surface was located in the middle of the bayonet tube (Fig. 1c). In this heating & measurement surface, a constant heat flux, over the time and the surface, was produced by Joule heating when an electric current passed through a stainless-steel film of negligible thickness (20 μm) which spans around 207° and forms the external tube wall in that region (light blue dashed-line in Fig. 1d). The total surface of this film was $7.1 \cdot 10^{-3}$ m² (14.5 × 4.9 cm, where the 14.5 cm includes the length along the outer tube, 9.75 cm, and an additional length, 4.75 cm, to fasten the metal foil to the assembly). The rest of the circumferential wall of the external tube in the axial location of the heating & measurement surface is formed by a 3-D printed plastic block (grey material in Fig. 1d). Note that there is no need to cover with the film the entire circumference of the tube because the measurement point is only affected by the foil within a narrow circumferential angle, since the air in the duct is principally advected in axial direction. On the top and bottom of the heating & measurement section, the external tube is adjusted in the red shaded area in Fig. 1d so that the smoothness of the surface in the annular section is maintained. The power supply (BK Precision 1900B, with a voltage and current resolution of 0.1 V and 0.1 A, respectively) to the stainless-steel film was homogeneously distributed using an indium wire in contact with the film (Fig. 1f). Additionally, the inner tube was mounted on a bottom disk that allowed rotation from 0 to 360° with respect to the central axis of the bayonet facility. Thus, when the inner tube was in an eccentric configuration, the position of the inner tube with respect to the heating and measurement surface was modified by rotating the bottom disk a given angle, $\theta$. To characterize how the position of the inner tube affects the convection heat transfer, a set of measurements for different angular positions was performed, from $\theta = 0°$ to $180°$, which represent the closest and farthest

positions of the inner tube to the measurement region, respectively. Results for angles greater than 180° are unnecessary on account of the symmetry of the system. The definition of the angular measured positions is shown in Fig. 2.

Several notches were used in the upper and bottom parts of the facility for a perfect positioning and alignment of the inner tube (Fig. 1e) for each angular measurement position $\theta$. The temperature data was acquired over the measurement region using an infrared camera (Optris PI400), with a temperature resolution of 0.1 °C. Prior to the experimental campaign, the camera was calibrated with a surface
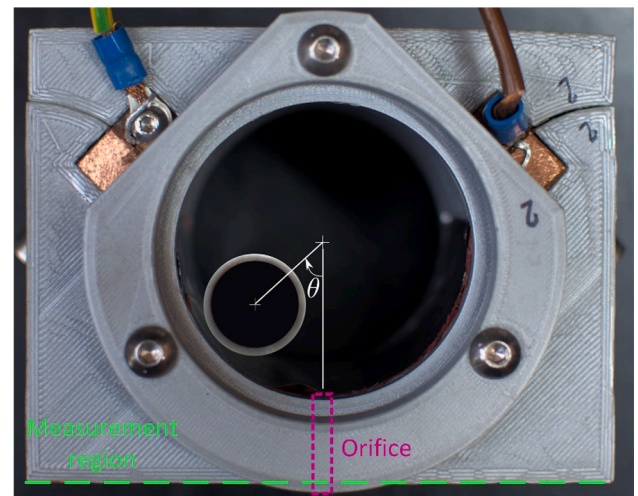


**Fig. 2.** Definition of the angular measurement position $\theta$.

thermocouple placed on the metal foil to adjust the software options and get reliable measurements. A 5 mm orifice ($d_{orifice}$, purple circle in Fig. 1c) was made in this region (solid grey block, indicated by the green dashed-line in Fig. 1c) to measure the temperature of the external surface of the stainless-steel film, which forms the wall of the external tube in that region. Air from a compressed air-line was used as a fluid, which entered through four orifices located in the bottom section of the bayonet tube and passed through a homogenization section which consisted of steel wool an aluminium honeycomb. The air flow rate was measured using a volume flow meter (SMC), with a flow resolution of 5 l/min. After passing the heating & measurement section, the air exited the tube through its upper end which was open to the ambient.

### 2.2. Experimental procedure

The inner tube was initially placed at the position $\theta = 180°$ (opposite to the measurement orifice) for an eccentricity of $\xi = 0.44$ and the air flow rate was set to a selected value to achieve a value of the Reynolds number, $Re_{Dh}$ ($10^4$, $2·10^4$ and $4·10^4$). In the definition of $Re_{Dh}$, the hydraulic diameter, $D_h$, is the characteristic length. The values of $Re_{Dh}$ were chosen to get a completely turbulent flow in the annular section to simulate usual conditions in industrial applications. The air temperature entering the bayonet heat exchanger was measured with a thermocouple with a resolution of 0.1°C, resulting in $T_{air} = 21°C$, and the infrared camera was fixed in a tripod to keep the same reference in all the measurements. Once the setup was ready, the power supply to the heating film was turned on with a voltage and a current equal to 10 V and 2 A, respectively, resulting in a homogeneous heat flux of $q'' = 2.9\text{kW/m}^2$. This heat flux can be considered to be dissipated by the film to the air in the annular section since thermal losses to the exterior are negligible on account of the reduced diameter of the measurement orifice and the low conductivity of the plastic material surrounding from outside the film. Just after turning on the heating film, the temperature in the measurement orifice was continuously measured by the infrared camera. When the temperature was stable and without changes, an image of the measurement region was saved. Fig. 3 shows a real image of the measurement region and the image acquired by the infrared camera described above. The measurement region is defined in Fig. 3a by a white dash line for an example case (nominal case at $Re_{Dh} = 2·10^4$). Fig. 3b shows the thermographic map resulting from the image processing results of the measurement region indicated in Fig. 3a. In Fig. 3b, an intense yellow colour in the orifice can be observed, which corresponds to the high temperature reached in the stainless-steel film. Subsequently, the power supply was turned off and the air flow rate was changed to the next $Re_{Dh}$ value to be studied. Once the initial temperature values in the whole measurement region were restored due to the

cooling produced by the air flow, the power supply was again turned on, repeating the process until measurements for all the $Re_{Dh}$ values were completed. Then, the inner tube was moved to the next position, 90°, and the whole procedure was repeated again. The measurements were done at the following positions and in decreasing order: 180°, 90°, 45°, 22.5° and 0°. As can be seen, a higher angle resolution was chosen in the vicinity of the measurement orifice. Additionally, the concentric position in the bayonet heat exchanger ($\xi = 0$) was also measured as reference case for the different $Re_{Dh}$ values. No angle variation was needed for the concentric configuration on account of its axis symmetry. Table 1 shows the experimental conditions and the measured temperatures. The temperature in the measurement orifice, $T_m$, was calculated as the spatially averaged value in the orifice region in the thermographic image ($2090 \pm 36$ pixels) and represents the temperature of the heating film at that position. The relation between the real and the image dimensions resulted in 1 mm corresponding to 10–11 pixels. The uncertainty of the measured and calculated values was evaluated by means of the propagation of uncertainty technique (see Supplementary Information). This uncertainty calculations are represented in the figures as error bars.

**Table 1**
Experimental conditions and results.

| $Re_{Dh}$ [–] | $\theta$ [°] | $T_m$ [°C] | $q''$ [W·m$^{-2}$] | $h_{exp}$ [W·m$^{-2}$·K$^{-1}$] | $Nu_{nd,exp}$ [–] |
|---|---|---|---|---|---|
| $10^4$ | Nominal | $35.0 \pm 0.1$ | $2740 \pm 143$ | $196 \pm 10$ | $239 \pm 14$ |
| $2·10^4$ | *Nominal* | $30.6 \pm 0.1$ | $2740 \pm 143$ | $285 \pm 15$ | $347 \pm 20$ |
| $4·10^4$ | *Nominal* | $28.6 \pm 0.1$ | $2712 \pm 142$ | $357 \pm 20$ | $434 \pm 26$ |
| $10^4$ | 0 | $39.6 \pm 0.1$ | $2996 \pm 149$ | $161 \pm 8$ | $196 \pm 11$ |
| $2·10^4$ | 0 | $36.5 \pm 0.1$ | $2966 \pm 148$ | $191 \pm 10$ | $232 \pm 13$ |
| $4·10^4$ | 0 | $32.5 \pm 0.1$ | $3055 \pm 152$ | $266 \pm 14$ | $324 \pm 18$ |
| $10^4$ | 22.5 | $38.8 \pm 0.1$ | $2966 \pm 148$ | $166 \pm 8$ | $202 \pm 11$ |
| $2·10^4$ | 22.5 | $35.9 \pm 0.1$ | $2996 \pm 149$ | $201 \pm 10$ | $244 \pm 14$ |
| $4·10^4$ | 22.5 | $31.8 \pm 0.1$ | $3055 \pm 152$ | $284 \pm 15$ | $345 \pm 19$ |
| $10^4$ | 45 | $36.9 \pm 0.1$ | $2996 \pm 149$ | $188 \pm 10$ | $229 \pm 13$ |
| $2·10^4$ | 45 | $34.8 \pm 0.1$ | $3055 \pm 152$ | $222 \pm 11$ | $270 \pm 15$ |
| $4·10^4$ | 45 | $31.1 \pm 0.1$ | $2910 \pm 151$ | $287 \pm 15$ | $349 \pm 20$ |
| $10^4$ | 90 | $35.5 \pm 0.1$ | $2996 \pm 149$ | $207 \pm 11$ | $252 \pm 14$ |
| $2·10^4$ | 90 | $32.9 \pm 0.1$ | $2996 \pm 149$ | $252 \pm 13$ | $307 \pm 17$ |
| $4·10^4$ | 90 | $30.3 \pm 0.1$ | $2910 \pm 151$ | $311 \pm 17$ | $379 \pm 22$ |
| $10^4$ | 180 | $33.6 \pm 0.1$ | $3055 \pm 152$ | $242 \pm 12$ | $295 \pm 16$ |
| $2·10^4$ | 180 | $29.5 \pm 0.1$ | $2966 \pm 148$ | $348 \pm 18$ | $423 \pm 24$ |
| $4·10^4$ | 180 | $28.0 \pm 0.1$ | $3025 \pm 151$ | $433 \pm 23$ | $527 \pm 31$ |
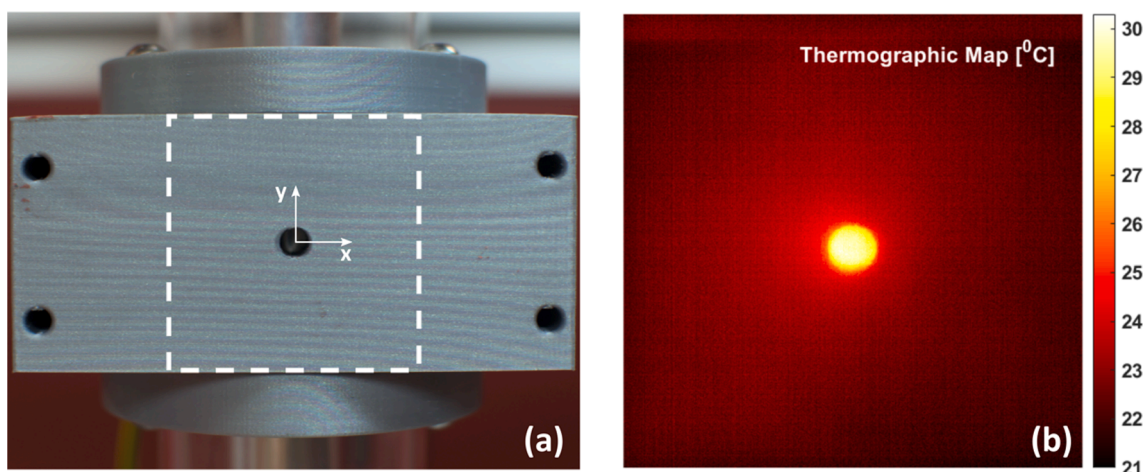


**Fig. 3.** Detail of the image acquisition process: a) measurement region and b) thermographic image.

## 3. Results and discussion

### 3.1. Temperature profiles

The acquired thermographic images for the nominal case (concentric tubes, $\xi = 0$) and the different $Re_{Dh}$ values are shown in Fig. 4. The mean temperature, $T_m$, of the orifice experienced an abrupt increase with regards the surrounding temperature because the orifice allowed the camera to capture the temperature of the heating film on the tube wall. This temperature adopts higher values for low $Re_{Dh}$ due to the lower turbulence and, hence, lower refrigeration capacity of the air in the annular duct. The reduced cooling rate for these conditions was also observed in the temperature of the zone surrounding the measurement orifice, though temperature changes in this surrounding zone were very limited because the low thermal conductivity of the plastic walls. The same trend with $Re_{Dh}$ was observed in the orifice temperatures for the eccentric annulus at the different angular positions.

An asymmetric temperature distribution along the axial direction is observed in the temperature profiles reported in Fig. 4. If the fluid velocity is reduced, the residence time of the fluid close to the heater grows, causing larger heating and this leads to a more noticeable temperature asymmetry between the bottom and top of the measuring orifice. Thus, the temperature asymmetry observed in Fig. 4, is emphasized as the fluid velocity decreases and mitigated as $Re_{Dh}$ grows.

For the eccentric annular section ($\xi = 0.44$), the effect of the angular position of the inner tube on the temperature $T_m$ of the measurement orifice is shown in Fig. 5, where the measurement uncertainty, calculated by means of the propagation of uncertainty technique (see Supplementary Information), is represented as error bars. As can be observed in the figure, the largest orifice temperature is found when the inner tube was closest to the orifice ($\theta = 0^o$). The narrow cross-section area for the air flow in the tube close to the measurement region
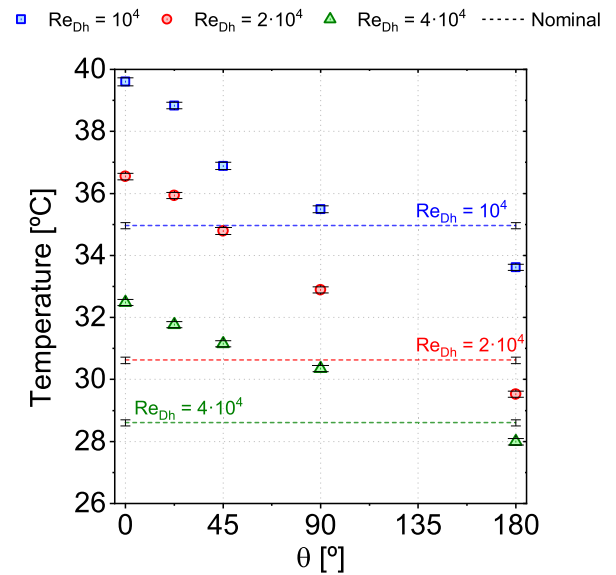


**Fig. 5.** Spatially averaged temperature, $T_m$, profile in the measurement orifice as a function of the angular position.

when $\theta = 0^o$ produces a restriction of the flow velocity, resulting in higher temperatures in the film. As the inner tube moves away from 0 to $180^o$, there is a reduction in the film temperature because the higher air flow in the proximity of the orifice produces a higher heat transfer rate between the air flow and the tube wall. As expected, the larger the Reynolds numbers, the greater cooling effect of the air in the wall of the measurement region and the lower temperatures $T_m$ were measured in
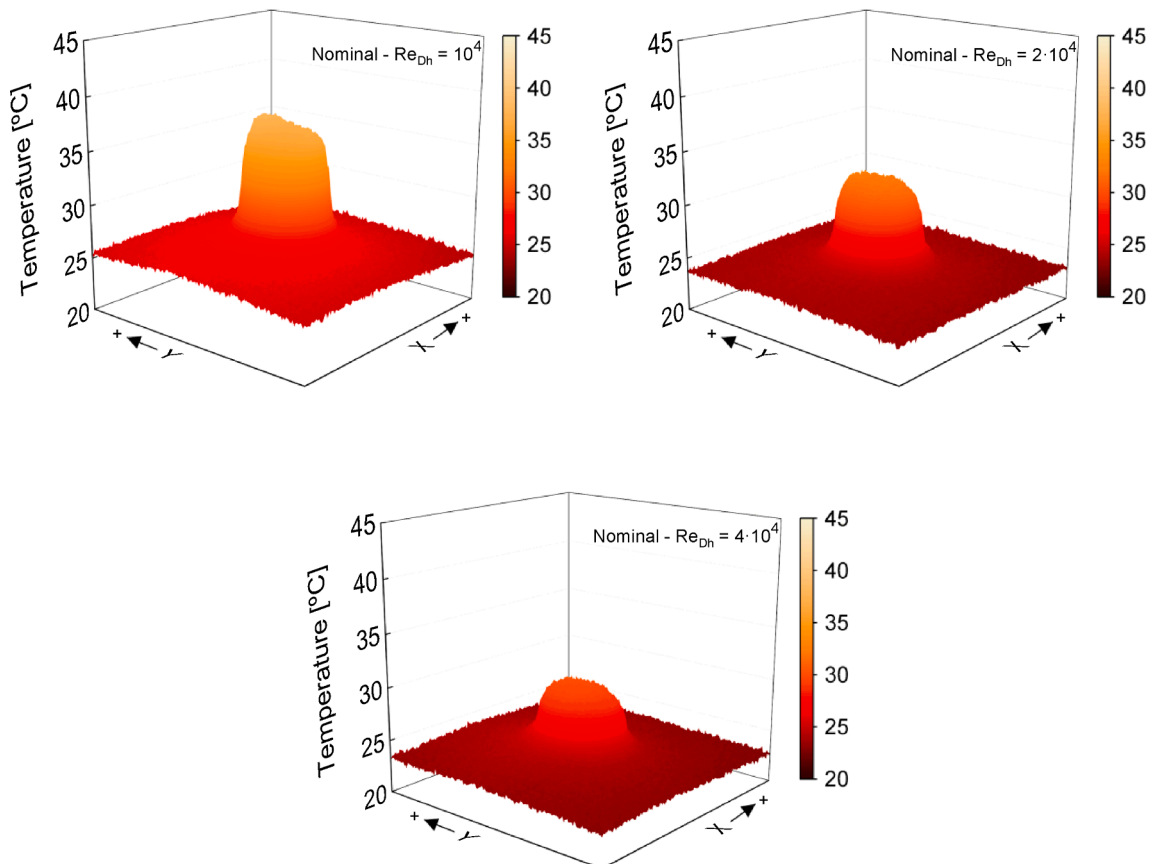


**Fig. 4.** Temperature profile in the orifice region measured for the nominal case (concentric annular section) at different values of $Re_{Dh}$.

the orifice.

When comparing the concentric annular duct (dotted lines in Fig. 5) with the eccentric one, it was found that differences between the concentric (nominal case) and eccentric temperatures in the orifice, $T_m$, tend to be small for $\theta$ between 90 and 180°, indicating that the effect of the inner tube position begins to become more relevant below 90°. However, the hydrodynamics and turbulent mixing behaviour of the local flow close to the inner surface of the external tube wall also varies significantly for angles between 90 and 180°.

### 3.2. Heat transfer coefficient and experimental correlation

The convection heat transfer coefficient was calculated to complete the analysis of the bayonet tube and improve the understanding of the circumferential distribution of the convective heat transfer inside an eccentric annular cross-section, a distribution rarely studied with experiments in the literature as mentioned before. Thus, the experimental local heat transfer coefficient, $h_{exp}$, was estimated from Newton's law of cooling as shown in Equation (1).

$$h_{exp}(\theta) = \frac{q^{''}(\theta)}{T_m(\theta) - T_{air}} \tag{1}$$

where $q^{''}$ is the incident heat flux dissipated by the aluminium film, $T_m$ is the mean tube temperature measured at the wall's orifice, and $T_{air}$ is the air temperature at the heat exchanger inlet. All these quantities, summarized in Table 1, depend on the experimental condition and the position of the inner bayonet tube, which is represented through $\theta$. Besides, the experiments carried out for the concentric configuration ($\xi = 0$) are named in Table 1 as nominal conditions. In Equation (1), the following assumptions are made: (i) on account of the good conductivity of the heating film, the temperature observed by the infrared camera, $T_m$, represents with a good degree of accuracy the surface temperature of the heating film on the side of the air flow in the annular tube; (ii) the bulk temperature of the air in the tube section where the measurements are undertaken is equal to $T_{air}$ because the film does not appreciably heat the air for the flow rates studied in this work.

The convection heat transfer coefficient inside the eccentric bayonet heat exchanger is not circumferentially uniform due to its geometrical configuration. Therefore, a global heat transfer coefficient might not be very representative of the local distribution of the convection heat transfer inside an eccentric annular duct. However, no previous correlations for the local convective coefficient were found in the literature for eccentric bayonet heat exchangers. Thus, an experimental correlation for this type of configuration is provided in this work. It should be noticed that the values of the convective coefficient here calculated are affected by the fact that the flow is not totally developed from the thermal point of view, since the size of the heating film is limited in the axial direction. Conceptually, this leads to larger convective coefficients than in fully developed flows. Nevertheless, as this affects all measurements equally, the obtained trends of the dependence of the convective coefficient with the angle and Reynolds number are expected to be correct.

The proposed correlation to model the local Nusselt number is shown in Equation (2). In particular, the correlation provides the local Nusselt number for the thermally non-developed conditions as a function of the operating conditions, fluid type and the geometric configuration. In the correlation, the effects of these parameters on the convective heat transfer are considered through a local Reynolds number:

$$Nu_{\theta,nd} = C \cdot Pr^b \cdot Re_\theta^a = C^{'} \cdot Re_\theta^a \tag{2}$$

where $Nu_{\theta,nd} = \frac{h_{\theta,nd}L_c}{k_{air}}$ is the local Nusselt number, which is evaluated with the local convection coefficient for thermally non-developed conditions, $h_{\theta,nd}$, at a circumferential position $\theta$ with regard the inner tube, $Pr$ is the Prandtl number of the working fluid, $C$ and $C^{'}$ are constants, the last one

englobing the effect of $Pr$, and $Re_\theta$ is the local Reynolds number, which is defined according to Equation (3):

$$Re_\theta = \frac{\rho_{air} u_\theta L_c}{\mu_{air}} \tag{3}$$

where $\rho_{air}$ and $\mu_{air}$ are the density and viscosity of the air, $u_\theta$ is the characteristic velocity of the fluid flow near the measurement orifice position (i.e. local bulk velocity) and $L_c$ is the characteristic length affecting this local bulk velocity. The properties of the air are evaluated at the film temperature, which is the mean value between the inlet air temperature and the local surface temperature, $T_m$.

Through some mathematical manipulations, it is possible to express the local Nusselt number correlation in Equation (2) as a function of overall variables, i.e. the hydraulic diameter ($D_h$) and the mean (bulk) fluid velocity ($u_m$):

$$Nu_{\theta,D_h,nd} = \frac{h_{\theta,nd}D_h}{k_{air}} = C^{'} \cdot \left(\frac{\rho_{air} u_m D_h}{\mu_{air}}\right)^a \cdot \left(\frac{u_\theta}{u_m}\right)^a \cdot \left(\frac{L_c}{D_h}\right)^{a-1} \tag{4}$$

Therefore:

$$Nu_{\theta,D_h,nd} = C^{'} \cdot Re_{D_h}^a \cdot \left(\frac{u_\theta}{u_m}\right)^a \cdot \left(\frac{L_c}{D_h}\right)^{a-1} \tag{5}$$

where $Re_{Dh} = \frac{\rho_{air} u_m D_h}{\mu_{air}}$ is the conventional bulk Reynolds number of the internal air flow based on the bulk velocity of the internal flow and the hydraulic diameter of the annular cross-section.

As previously mentioned, $u_\theta$ and $L_c$ depend on the studied position of the inner tube. Owing to the non-symmetric behaviour of the fluid inside an annular cross-section, the detailed analytical characterization of these magnitudes is not straightforward. Only symmetry at $\theta = 0°$ and 180° of velocities and temperatures can result from the eccentric annular geometry. For this reason, these variables have been grouped and modelled as a polynomic cosine function, whose coefficients ($\alpha_1$, $\alpha_2$, …,$\alpha_n$) can be obtained through the experimental data fitting:

$$f(\theta) = \left(\frac{u_\theta}{u_m}\right)^a \cdot \left(\frac{L_c}{D_h}\right)^{a-1} = 1 + \alpha_1 \cdot cos(\theta) + \alpha_2 \cdot cos^2(\theta) + \cdots + \alpha_n \cdot cos^n(\theta) \tag{6}$$

It should be noticed that the experimental value of the local convective heat transfer coefficient calculated with Equation (1) has been obtained for non-fully developed conditions since the heating region is not large enough to allow the thermal and hydrodynamical development of the fluid ($L_{heated}/D_h = 1.53 < 10$). Thus, a correction of Equation (5) is done to estimate the fully developed local Nusselt number in the eccentric annular section from the value for the thermally non-developed local Nusselt number, $Nu_{\theta,D_h,nd}$:

$$Nu_{\theta,D_h(exp)} = \frac{Nu_{conc,D_h}}{Nu_{conc,D_h,nd}} \cdot Nu_{\theta,Dh,nd} \tag{7}$$

where $Nu_{\theta,D_h(exp)}$ is the fully developed local Nusselt number in the eccentric annular section estimated through a correction of the experimental results, $Nu_{conc,D_h}$ is a reference Nusselt number of a fully developed turbulent flow in the concentric annular section configuration, $Nu_{conc,D_h,nd}$ is the Nusselt number of the thermally non-developed flow of the experiment in the concentric annular section configuration ($Nu_{nd,exp}$ for the nominal case in Table 1), and $Nu_{\theta,D_h,nd}$ is the value for the thermally non-developed local Nusselt number experimentally determined in the eccentric cross-section ($Nu_{nd,exp}$ for the eccentric cases in Table 1). It is interesting to note that the fraction of non-developed Nusselt numbers in Equation (7), $\frac{Nu_{\theta,Dh,nd}}{Nu_{conc,D_h,nd}}$, is a weak function of the fully developed length of the annular tube (due to cancellation of the entry length dependence between numerator and denominator). Therefore, the value of the fraction $\frac{Nu_{\theta,Dh,nd}}{Nu_{conc,D_h,nd}}$ is applicable for the developed and non-

developed regions. More specifically, the Nusselt number correlation provided by Monrad and Pelton [30] is employed to calculate the reference Nusselt number $Nu_{conc,D_h}$, since they analysed a concentric annular section with an internal flow of air in turbulent conditions applicable to those of studied in the present work, where $a$ is the relation between the diameters of the external and internal tubes of the annular duct:

$$Nu_{conc,D_h} = 0.023 \left[ \frac{2 \ln a - a^2 + 1}{a - \frac{1}{a} - 2a \ln a} \right] Re_{D_h}^{0.8} Pr^{0.4} \tag{8}$$

Besides, the experiments carried out for the concentric configuration ($\xi = 0$) can be employed to determine the Nusselt number for a thermally non-developed flow, $Nu_{conc,D_h,nd}$, using Equation (1) with the experimental data for nominal conditions (concentric annular section), which leads to the $Nu_{exp}$ data in Table 1. Thus, for a given fluid and diameter ratio of the inner and outer tubes of the annular section, the fraction $\frac{Nu_{conc,D_h}}{Nu_{conc,D_h,nd}}$ in Equation (7) depends on the thermally non-developed conditions and the Reynolds number, which can be expressed as a power function of $Re_{Dh}$. Therefore, the following overall dependence is proposed:

$$Nu_{\theta,D_h} = C'' \cdot Re_{D_h}^b \cdot \left( 1 + \alpha_1 \cdot \cos(\theta) + \alpha_2 \cdot \cos^2(\theta) + \cdots + \alpha_n \cdot \cos^n(\theta) \right) \tag{9}$$

where $C''$, $b$ and $\alpha_i$ ($i = 1, \cdots, n$) are unknown coefficients to be obtained with the experimental data.

Several values of $n$ were tested to find the best fitting of Equation (9) with the values of $Nu_{\theta,D_h(exp)}$ calculated with the correction of the experimental data in Equation (7). The discrepancy between the Equation (9) and $Nu_{\theta,D_h(exp)}$, which is defined as $\delta = |Nu_{\theta,D_h} - Nu_{\theta,D_h(exp)}| / Nu_{\theta,D_h(exp)}$, slightly decreases with the grade of the polynomial function, achieving, for a polynomial function of second grade, a discrepancy below 10.0%. The discrepancy decreases to 7.6% when the function is a polynomial of fourth grade. For simplicity, a polynomial expression of second grade has been chosen for the experimental fitting ($\delta = 9.97\%$ and $R^2 = 0.988$), since its variation with respect to the polynomial expression of the fourth grade is irrelevant and the expression of second grade is simpler. In the light of the above considerations, the proposed correlation for the fully developed local Nusselt number of a turbulent flow of air in a smooth eccentric annular duct, with $\frac{d_e}{D_i} = 0.407$ and $\xi = 0.44$, is given by:

$$Nu_{\theta,D_h} = 0.0343 \cdot Re_{D_h}^{0.768} \cdot \left( 1 - 0.2507 \cdot \cos(\theta) + 0.0923 \cdot \cos^2(\theta) \right) \tag{10}$$

Note that the exponent of the Reynolds number in Equation (10), $b = 0.768$, is close to the value of 0.8, which is the exponent typically used in the Nusselt number correlations for a turbulent flow in a duct.

Fig. 6 shows the variation of the fully developed local Nusselt number convection with the circumferential angle position relative to the inner tube for different $Re_{Dh}$ of the air flow. The local Nusselt number increases with the angle position, from $0^o$ to $180^o$. This fact is caused by the growth of the local fluid velocity with $\theta$, which is translated into an enhancement of the local convection heat transfer in the region of the measurement orifice. For low $Re_{Dh}$, the increment of $Nu_{\theta,D_h}$ with $\theta$ is rather linear while for higher values ($2 \cdot 10^4$ and $4 \cdot 10^4$) a sharper increment is noticed. This increment is moderate from $0^o$ to $90^o$ while it is emphasized from $90^o$ to $180^o$, the effect being more noticeable for higher $Re_{Dh}$. The Nusselt number for the nominal case results to be rather similar to that of the eccentric case obtained for $90^o$ ($Re_{Dh} = 10^4$), but this similarity shifts to higher values of $\theta$, between $90^o$ and $180^o$, when the $Re_{Dh}$ is increased. In Fig. 6, the maximum discrepancy between the correlation (Equation (10)) and the corrected empirical data ($\delta = 9.97\%$) is obtained for $Re_{Dh} = 10^4$ at $\theta = 45^o$. As was reported in the literature [31] the effect of the thermal entrance region is to increase the heat transfer rate and/or Nusselt number compared to that for thermally
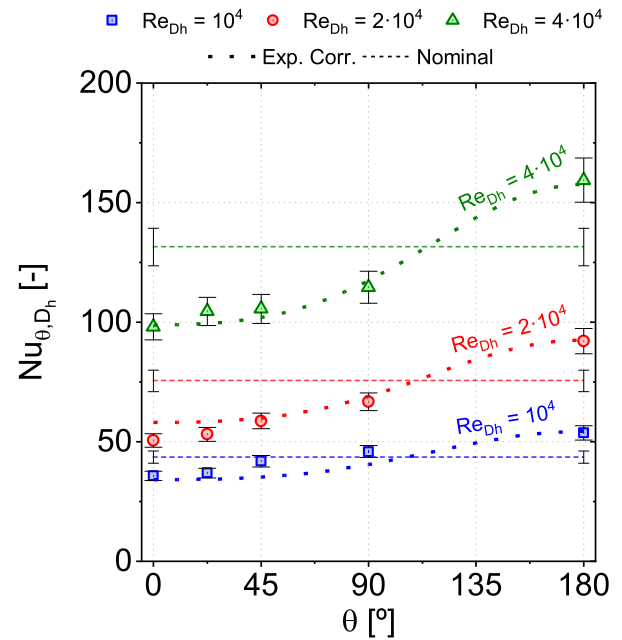


**Fig. 6.** Fully developed local Nusselt number as a function of the angular position and the bulk Reynolds number.

developed flow. This fact justifies the difference between values reported in Table 1 and those illustrated in Fig. 6, where the former was obtained for non-fully developed flow, while the latter were obtained for fully developed conditions.

The results of Equation (10) for predicting the fully developed local Nusselt number experimentally estimated in this work is compared in Table 2 with other correlations proposed in the literature, which were developed to estimate the convection coefficient of uniformly heated concentric passages. The results summarized in the table have been calculated for the conditions (i.e., same dimensions of the tube and fluid properties where the diameters relation was defined as $a = D_i/d_e$) analysed in the present work. As the correlation proposed in this work depends on the position of the inner tube, the extreme values (i.e. $\theta = 0^o$ and $\theta = 180^o$) have been provided in the table for this case. As was reported by Pérez-Álvarez et al. [32], the eccentricity of the bayonet tube enhances the convection heat transfer. This fact explains the difference with the values of the correlations for concentric tubes reported by other authors.

## 4. Conclusions

The local convective heat transfer coefficient of the outer tube in the annular section of an eccentric annular duct was experimentally evaluated for different circumferential positions relative to the inner tube and for several turbulent flow Reynolds numbers. The results indicated that the eccentricity of the inner tube, clearly influences the distribution of the convective coefficient. In particular, the perturbation of the eccentric tube on the hydrodynamics of the flow seem to produce a growth of the convection coefficient from an angular position equal to $\theta = 0^o$, (internal tube at its closest position to the measurement point) to $180^o$ (internal tube opposite to the measurement point). Higher temperatures were obtained for $0^o$ due to the lower refrigeration capacity of the low at this circumferential position for all $Re_{Dh}$, implying lower convection coefficients. The experimental results clearly indicated that the convective coefficient for the nominal concentric cases were inferior than the local convective coefficient for the eccentric cases in a region of circumferential positions between $90^o$ and $180^o$, showing the benefits, in heat transfer terms, of the eccentricity configurations. Based on the experimental results, a correlation of the local Nusselt number of a

**Table 2**
Comparison of the Nusselt number values obtained with the correlation presented in this work and correlation available in the literature for $a = 2.45$.

| Authors (Type of tube) | Expression | $Re_{D_h}$ | | |
|---|---|---|---|---|
| | | $10^4$ | $2\cdot10^4$ | $4\cdot10^4$ |
| Present work (Eccentric, $\xi = 0.5$) | $Nu = 0.0343\cdot Re_{D_h}^{0.768}\cdot(1 - 0.2507\cdot cos(\theta) + 0.0923\cdot cos^2(\theta))$ | $34-55$ | $58-93$ | $99-158$ |
| Monrad and Pelton [30] (Concentric) | $Nu = 0.023\left[\dfrac{2\ ln\ a - a^2 + 1}{a - \frac{1}{a} - 2a\ ln\ a}\right]Re_{D_h}^{0.8}Pr^{0.4}$ | 36 | 62 | 108 |
| Dittus and Boelter [33] (Concentric) | $Nu = 0.023Re^{0.8}Pr^{\frac{1}{3}}$ | 26 | 45 | 79 |
| Stein and Begell [34] (Concentric) | $Nu = 0.02a^{0.5}Re^{0.8}Pr^{\frac{1}{3}}$ | 36 | 63 | 110 |
| Crookston et al. [35] (Concentric) | $Nu = 0.023a^{0.25}Re^{0.75}Pr^{\frac{1}{3}}$ | 21 | 35 | 60 |
| Foust and Christian [36] (Concentric) | $Nu = 0.04\dfrac{a}{(a+1)^2}Re^{0.8}Pr^{0.4}$ | 87 | 151 | 263 |

turbulent flow of air in an eccentric annular tube was proposed. The proposed experimental correlation reproduced with relatively high accuracy the fully developed conditions inferred from the experimental data for the different positions and turbulent Reynolds number studied in this work.

## Declaration of Competing Interest

The authors declare that they have no known competing financial interests or personal relationships that could have appeared to influence the work reported in this paper.

## Acknowledgements

## Appendix A. Supplementary material

Supplementary data to this article can be found online at https://doi.org/10.1016/j.expthermflusci.2022.110664.

## References

[1] H.K. Dawood, H.A. Mohammed, N.A. Che Sidik, K.M. Munisamy, M.A. Wahid, Forced, natural and mixed-convection heat transfer and fluid flow in annulus: A review, Int. Commun. Heat Mass Transf. 62 (2015) 45–57, https://doi.org/10.1016/J.ICHEATMASSTRANSFER.2015.01.006.
[2] M.H. Farias, C.V.M. Braga, P.R. de Souza Mendes, Heat transfer coefficients for the laminar fully developed flow of viscoplastic liquids through annuli, Int. J. Heat Mass Transf. 52 (13–14) (2009) 3257–3260, https://doi.org/10.1016/J.IJHEATMASSTRANSFER.2009.02.008.
[3] K. Chen, C. Yan, Z. Meng, X. Wu, S. Song, Z. Yang, J. Yu, Experimental analysis on passive residual heat removal in molten salt reactor using single cooling thimble test system, Energy. 112 (2016) 1049–1059, https://doi.org/10.1016/J.ENERGY.2016.07.004.
[4] F. Giannetti, D. Vitale Di Maio, A. Naviglio, G. Caruso, Thermal-hydraulic analysis of an innovative decay heat removal system for lead-cooled fast reactors, Nucl. Eng. Des. 305 (2016) 168–178, https://doi.org/10.1016/J.NUCENGDES.2016.05.005.
[5] L. Damiani, M. Montecucco, A. Pini Prato, Conceptual design of a bayonet-tube steam generator for the ALFRED lead-cooled reactor, Nucl. Eng. Des. 265 (2013) 154–163, https://doi.org/10.1016/J.NUCENGDES.2013.06.021.
[6] S. Tang, Z. Liang, G.H. Zhao, Dynamic stability of lateral vibration of a tubing string in flowing production, J. Vibroengineering. 20 (7) (2018) 2540–2549, https://doi.org/10.21595/JVE.2018.18989.
[7] J.D. Morris, E.B. Diethrich, PRESSURE-PERFUSION CANNULA: A simplified method of monitoring central arterial pressure during perfusion, J. Thorac. Cardiovasc. Surg. 43 (6) (1962) 822–824, https://doi.org/10.1016/S0022-5223(19)33023-5.
[8] G.S.H. Lock, H. Minhas, Bayonet tube heat exchanger, Appl. Mech. Rev. 50 (1997) 445–473, https://doi.org/10.1115/1.3101733.
[9] S. Fukusako, N. Seki, M. Yamada, Heat-removal characteristics of a combined system of concentric-tube thermosyphon and heat pump: heat transfer, power, combustion, thermophysical properties, JSME Int. J. 30 (264) (1987) 936–944, https://doi.org/10.1299/JSME1987.30.936.
[10] K. Khanafer, A. Al-Amiri, I. Pop, Numerical analysis of natural convection heat transfer in a horizontal annulus partially filled with a fluid-saturated porous substrate, Int. J. Heat Mass Transf. 51 (7–8) (2008) 1613–1627, https://doi.org/10.1016/J.IJHEATMASSTRANSFER.2007.07.050.
[11] P.V. Reddy, G.S.V.L. Narasimham, Natural convection in a vertical annulus driven by a central heat generating rod, Int. J. Heat Mass Transf. 51 (19–20) (2008) 5024–5032, https://doi.org/10.1016/J.IJHEATMASSTRANSFER.2008.02.032.
[12] R. Ben Radhia, J.P. Corriou, S. Harmand, S. Ben Jabrallah, Numerical study of evaporation in a vertical annulus heated at the inner wall, Int. J. Therm. Sci. 50 (10) (2011) 1996–2005, https://doi.org/10.1016/J.IJTHERMALSCI.2011.03.007.
[13] X.u. Xu, G. Sun, Z. Yu, Y. Hu, L. Fan, K. Cen, Numerical investigation of laminar natural convective heat transfer from a horizontal triangular cylinder to its concentric cylindrical enclosure, Int. J. Heat Mass Transf. 52 (13–14) (2009) 3176–3186, https://doi.org/10.1016/J.IJHEATMASSTRANSFER.2009.01.026.
[14] J.L.V. Neto, A.L. Martins, A.S. Neto, C.H. Ataíde, M.A.S. Barrozo, CFD applied to turbulent flows in concentric and eccentric annuli with inner shaft rotation, Can. J. Chem. Eng. 89 (2011) 636–646, https://doi.org/10.1002/CJCE.20522.
[15] O.A. Alawi, N.A.C. Sidik, H.K. Dawood, Natural convection heat transfer in horizontal concentric annulus between outer cylinder and inner flat tube using nanofluid, Int. Commun. Heat Mass Transf. 57 (2014) 65–71, https://doi.org/10.1016/J.ICHEATMASSTRANSFER.2014.07.001.
[16] E. Abu-Nada, Effects of variable viscosity and thermal conductivity of Al2O3–water nanofluid on heat transfer enhancement in natural convection, Int. J. Heat Fluid Flow. 30 (4) (2009) 679–690, https://doi.org/10.1016/J.IJHEATFLUIDFLOW.2009.02.003.
[17] M. Kaneda, B.o. Yu, H. Ozoe, S.W. Churchill, The characteristics of turbulent flow and convection in concentric circular annuli. Part I: flow, Int. J. Heat Mass Transf. 46 (26) (2003) 5045–5057, https://doi.org/10.1016/S0017-9310(03)00365-X.
[18] B.o. Yu, B. Kawaguchi, M. Kaneda, H. Ozoe, S.W. Churchill, The computed characteristics of turbulent flow and convection in concentric circular annuli. Part II. Uniform heating on the inner surface, Int. J. Heat Mass Transf. 48 (3–4) (2005) 621–634, https://doi.org/10.1016/J.IJHEATMASSTRANSFER.2004.08.022.
[19] N. Nikitin, H. Wang, S. Chernyshenko, Turbulent flow and heat transfer in eccentric annulus, J. Fluid Mech. 638 (2009) 95–116, https://doi.org/10.1017/S002211200900812X.
[20] M.R.H. Nobari, A. Asgarian, A numerical investigation of flow and mixed convection inside a vertical eccentric annulus, Numer. Heat Transf. Part A Appl. 55 (1) (2008) 77–99, https://doi.org/10.1080/10407780802603105.
[21] H.A. Mohammed, A. Campo, R. Saidur, Experimental study of forced and free convective heat transfer in the thermal entry region of horizontal concentric annuli, Int. Commun. Heat Mass Transf. 37 (7) (2010) 739–747, https://doi.org/10.1016/J.ICHEATMASSTRANSFER.2010.04.007.
[22] W.S. Kim, C. Talbot, B.J. Chung, J.D. Jackson, Variable property mixed convection heat transfer to air flowing through a vertical passage of annular cross section: Part 1, Chem. Eng. Res. Des. 80 (3) (2002) 239–245, https://doi.org/10.1205/026387602753581999.
[23] J. Dirker, J.P. Meyer, Convective heat transfer coefficients in concentric annuli, Heat Transf. Eng. 26 (2) (2005) 38–44, https://doi.org/10.1080/01457630590897097.
[24] V. Gnielinski, Heat transfer coefficients for turbulent flow in concentric annular ducts, Heat Transf. Eng. 30 (6) (2009) 431–436, https://doi.org/10.1080/01457630802528661.
[25] V.K. Jonsson, E.M. Sparrow, Experiments on turbulent-flow phenomena in eccentric annular ducts, J. Fluid Mech. 25 (1) (1966) 65–86, https://doi.org/10.1017/S0022112066000053.
[26] J.M. Nouri, H. Umur, J.H. Whitelaw, Flow of Newtonian and non-Newtonian fluids in concentric and eccentric annuli, J. Fluid Mech. 253 (1993) 617–641, https://doi.org/10.1017/S0022112093001922.

[27] G.H. Choueiri, S. Tavoularis, Experimental investigation of flow development and gap vortex street in an eccentric annular channel. Part 1. Overview of the flow structure, J. Fluid Mech. 752 (2014) 521–542, https://doi.org/10.1017/JFM.2014.343.

[28] G.H. Choueiri, S. Tavoularis, Experimental investigation of flow development and gap vortex street in an eccentric annular channel. Part 2. Effects of inlet conditions, diameter ratio, eccentricity and Reynolds number, J. Fluid Mech. 768 (2015) 294–315, https://doi.org/10.1017/JFM.2015.90.

[29] R. Hosseini, M.R. Heyrani-Nobari, M. Hatam, An experimental study of heat transfer in an open-ended vertical eccentric annulus with insulated and constant heat flux boundaries, Appl. Therm. Eng. 25 (8–9) (2005) 1247–1257, https://doi.org/10.1016/J.APPLTHERMALENG.2004.08.016.

[30] C.C. Monrad, J.F. Pelton, Heat transfer by convection in annular spaces, Trans. Am. Inst. Chem. Engieneers. 38 (1942) 593–611.

[31] R.K. Shah, A.L. London, Laminar Flow Forced Convection in Ducts: A Source Book for Compact Heat Exchanger Analytical Data, Academic Press, 1978.

[32] R. Pérez-Álvarez, M.R. Rodríguez-Sánchez, A. Acosta-Iborra, D. Santana, Effect of eccentricity on the hydrodynamics and heat transfer of molten salt in bayonet receivers for solar power towers, AIP Conf. Proc. 2033 (2018), 080004, https://doi.org/10.1063/1.5067093.

[33] F.W. Dittus, L.M.K. Boelter, Heat Transfer in Automobile Radiators of the Tubular Type, University of California Press, Berkeley Calif., 1930.

[34] R.P. Stein, W. Begell, Heat transfer to water in turbulent flow in internally heated annuli, AIChE J. 4 (2) (1958) 127–131, https://doi.org/10.1002/AIC.690040203.

[35] R.B. Crookston, R.R. Rothfus, R.I. Kermode, Turbulent heat transfer in annuli with small cores, Int. J. Heat Mass Transf. 11 (3) (1968) 415–426, https://doi.org/10.1016/0017-9310(68)90086-0.

[36] A.S. Foust, G.A. Christian, Non-boiling heat transfer coefficients in annuli, Am. Inst. Chem. Eng. 36 (1940) 541–554.